

Highly Active Ir/TiO₂ Electrodes for the Oxygen Evolution Reaction Using Atomic Layer Deposition on Ordered Porous Substrates

Stefanie Schlicht,[†] Pascal Büttner,[†] and Julien Bachmann^{*,†,‡,§}

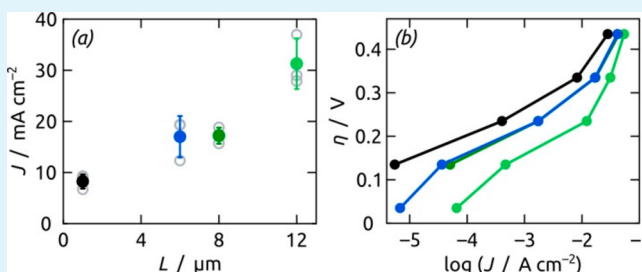
[†]Department of Chemistry and Pharmacy, Friedrich-Alexander University Erlangen-Nürnberg, IZNF, Cauerstraße 3, 91058 Erlangen, Germany

[‡]Institute of Chemistry, Saint-Petersburg State University, Universitetskii Prospekt, 26, 198504 St. Petersburg, Russia

S Supporting Information

ABSTRACT: Nanostructured Ir/TiO₂ electrodes are investigated toward the oxygen evolution reaction (OER) from water. The electrodes are prepared based on highly ordered TiO₂ nanotubes grown from Ti foils with full geometric control. The tube walls are coated with iridium using atomic layer deposition (ALD), which allows for an accurate tuning of the amount deposited. The electrocatalytic performance of electrodes with different TiO₂ tube lengths and iridium catalyst loadings toward OER is quantified by cyclic voltammetry and steady-state electrolysis. This study enables us to minimize the catalyst loading, and we reach a current density of 31.3 mA cm⁻² at an overpotential η = 0.34 V for a tube length of L = 12 μ m and a Ir coating thickness of t = 6 nm. The benchmark of 10 mA cm⁻² is already achieved at a lower overpotential of η = 0.24 V.

KEYWORDS: oxygen evolution reaction, titania nanotubes, iridium, atomic layer deposition, nanostructuring



INTRODUCTION

Renewable energy sources such as solar or wind power are indispensable nowadays. Due to their intermittent availability, energy storage and release systems such as electrolyzers and fuel cells have become a crucial topic of academic research and industrial development.^{1,2} In order to generate hydrogen (the chemical energy storage media) and oxygen from water, electrolyzers such as proton exchange membrane (PEM) cells are needed. The electrochemical splitting of water into its elements is kinetically limited by the positive electrode reaction, the four-electron evolution of dioxygen. To overcome this issue, an electrode presenting an effective catalyst material in accessible geometry is needed. The oxidized surfaces of the noble metals Ru and Ir are currently considered the best electrocatalysts toward the oxygen evolution reaction due to their high activity and (for Ir) stability.^{3,4} The high price and scarcity of these catalysts prompt a strong interest in minimizing their loading.⁵

Optimizing the electrode geometry represents an attractive strategy to improving the slow kinetics with minimized noble metal loadings. Nanostructured substrates such as anodic aluminum oxide provide well-ordered, straight, cylindrical nanopores and allow for the systematic tuning of the electrode geometric surface area.^{6,7} This substrate is limited by its nonconductive nature and must be coated with a thick, continuous layer of (noble) metal to ensure electrical transport.⁷ Anodic titanium dioxide nanotube arrays as an electrically conductive substrate represent an attractive alternative. This advantage combined with their high surface-

to-volume ratio and the precise control of their geometry (Table 1) has rendered them a template of choice in energy

Table 1. Ratio between Microscopic Surface Area and Macroscopic Sample Area (“Roughness Factor”) Calculated Based on the Geometric Parameters (Pore Length and Number of ALD Cycles) for Some Representative Porous Samples

	0 cycle	75 cycles	250 cycles
6 μ m	190	170	120
8 μ m	260	230	160
12 μ m	380	340	240

conversion and storage applications such as water electrolysis and photoelectrolysis, photocatalysis, or solar cells.^{8–11} Additional features of TiO₂ are its mechanical and chemical stability, low toxicity, environmentally benign character, and corrosion resistance.¹²

Herein, we present a method to reduce the electrodes' catalyst loading using atomic layer deposition. This technique allows for the conformal coating of highly porous substrates, whereas the amount deposited can be tuned accurately. We investigate the electrochemical performance of ordered TiO₂ nanotubes coated with iridium toward the oxygen evolution

Received: February 26, 2019

Accepted: February 28, 2019

Published: February 28, 2019

reaction. The performance depends on the geometry of the electrodes systematically. Finally, we minimize the noble metal loading in order to lower the material costs for electrode fabrication.

RESULTS AND DISCUSSION

Preparation and Characterization. Our nanostructured electrodes are prepared by growing TiO_2 nanotube arrays from Ti foils in a fluoride-containing electrolyte. Figure 1a–c

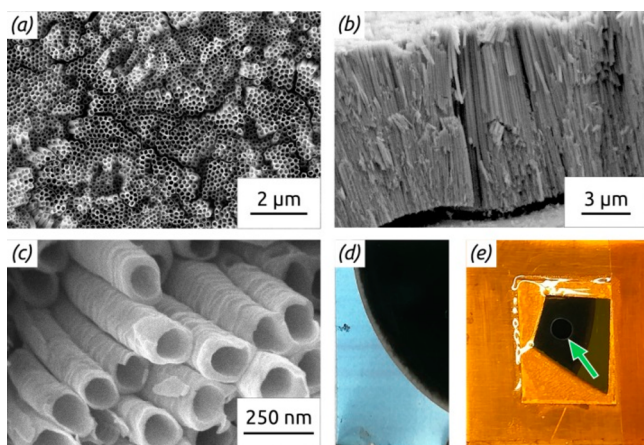


Figure 1. Scanning electron micrographs of anodic TiO_2 nanotubes grown from Ti foil in 0.5 wt % NH_4F containing ethylene glycol for 3 h in top view (a) and cross section (b, c). (d) Photograph of a sample after coating with iridium by atomic layer deposition. (e) Sample for electrochemical investigations. A piece is glued on a Cu plate using Cu tape and masked with Kapton tape with circular opening of $d = 2.0$ mm (green arrow).

displays scanning electron micrographs of the TiO_2 nanotubes from the top view and in cross section, respectively. The electrochemical oxidation (anodization) leads to the formation of self-organized and well-ordered nanotubes. The geometry can be modified by varying the length of the nanotubes depending on the anodization duration. In our anodization conditions in ethylene glycol, anodization times of 1, 2, and 3 h result in TiO_2 tube lengths of $L \approx 6 \mu\text{m}$, $L \approx 8 \mu\text{m}$, and $L \approx 12 \mu\text{m}$, respectively. Tubes shorter than $4 \mu\text{m}$ must be prepared in glycerol for them to feature on open extremity (Supporting Information Figure S1). The pore length translates into an increased specific surface area linearly, and “roughness factors” (ratio of microscopic surface area to macroscopic sample area) on the order of 100 to 400 are obtained (Table 1). These values calculated based on geometric parameters are in accordance with numbers determined from the capacitive currents in cyclic voltammetry, given roughness effects. As an example, a circular sample of 2 mm diameter with $12 \mu\text{m}$ long tubes and 75 ALD cycles has a macroscopic area of 0.0314 cm^2 and microscopic value of 10.7 cm^2 . For this sample, we measure an integrated capacitive current of 3.59 mC over one cyclic voltammogram, or a capacity of 2.99 mF . With an approximate double layer thickness of 8.77 \AA (Debye–Hückel), this capacity corresponds to 38 cm^2 . To improve the electrical conductivity, the originally amorphous TiO_2 tubes are annealed in air for 4 h at 450°C in order that they crystallize in the anatase phase (Figure 2). The resistance of a substrate with 2 mm macroscopic diameter determined with a simple two-contact measurement was 154Ω .

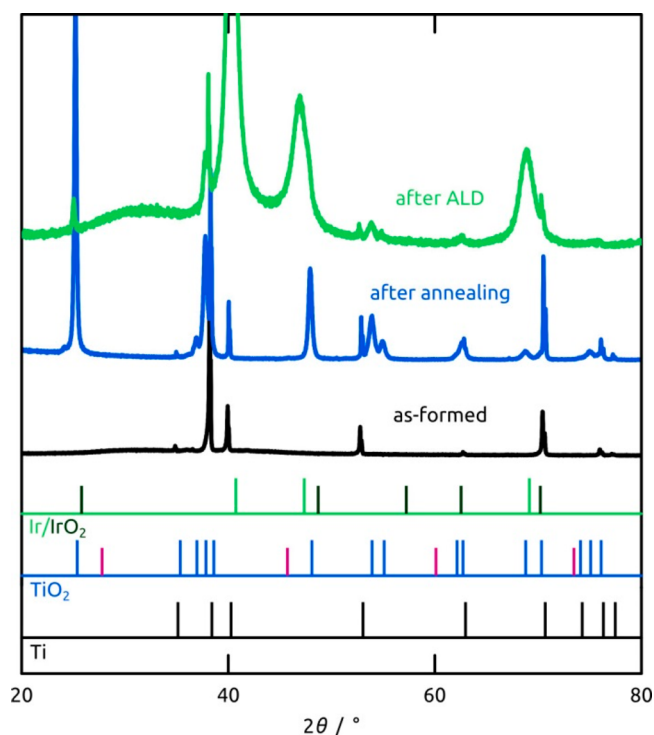


Figure 2. X-ray diffraction pattern of the TiO_2 nanotubes as formed (black), after annealing in air at 450°C for 4 h (blue), and after coating with iridium by atomic layer deposition. The corresponding standard pattern is given at the bottom for Ti (black), TiO_2 (anatase, blue; rutile, violet), Ir/IrO₂ (light green, dark green).

Finally, the tubes are coated with iridium by atomic layer deposition (ALD, from $(\text{EtCp})\text{Ir}(\text{CHD}) + \text{O}_3$ at 220°C).⁷ ALD enables a systematic control of the amount deposited. The chemical identity of the ALD deposit transpires in X-ray diffraction (XRD). The XRD pattern shows broad peaks consistent with nanocrystalline metallic Ir at $2\theta \approx 40^\circ$, $2\theta \approx 46^\circ$, and $2\theta \approx 68^\circ$ (attributed to the (111), (200), and (220) reflexes, COD 9008470).^{13,14} Energy-dispersive X-ray analysis exhibits signals for the expected elements Ti, O, and Ir (Figure 3). The photographs in Figure 1d,e show the sample after the coating with iridium by atomic layer deposition and after preparation for the electrochemical investigations. The black color along the whole sample surface indicates the formation of metallic iridium.

Electrocatalytic Performance toward Oxygen Evolution Reaction. The electrocatalytic activity toward oxygen evolution reaction (OER) of our nanostructured electrodes is investigated in acidic media by cyclic voltammetry (CV) and steady-state electrolysis. Let us first highlight the effect of the anodization and the ALD coating shown in the cyclic voltammograms in Figure 4. The electrodes of an untreated Ti foil (black curve) and an anodized Ti foil (blue curve) yield low current densities in the range of $\mu\text{A cm}^{-2}$. The CV curve of a planar Ti foil coated with iridium displays the exponential increase of the current density up to $J = 15 \text{ mA cm}^{-2}$ (at $+1.4 \text{ V}$ versus Ag/AgCl), resulting from the evolution of dioxygen from water (dark green curve). The light green CV curve now shows the effect of the high surface area of the TiO_2 nanotubes and the impact of the iridium catalyst. When anodization is complemented by ALD coating, the OER current increases up to $J \approx 70 \text{ mA cm}^{-2}$ at $+1.4 \text{ V}$ versus Ag/AgCl . Furthermore,

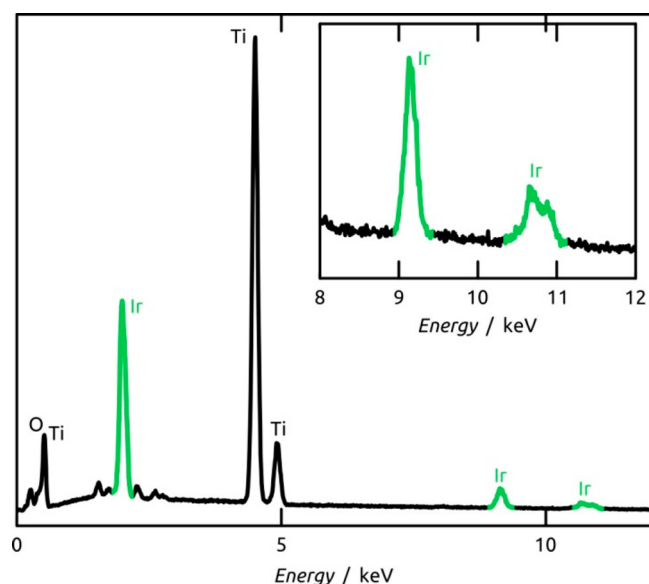


Figure 3. Energy-dispersive X-ray analysis of a coated sample proving the presence of the catalyst material.

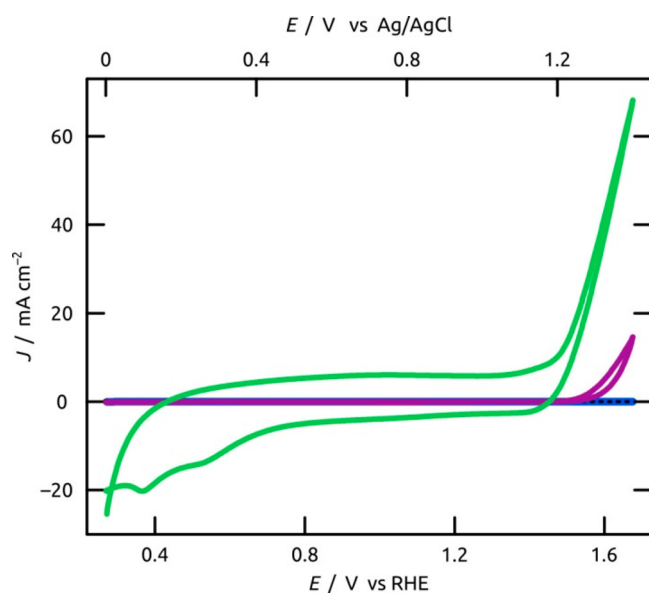


Figure 4. Cyclic voltammetry of electrodes with different treatments recorded in acidic media: untreated Ti foil (black, dashed), anodized Ti foil (blue), Ir-coated Ti foil (not anodized, purple), and anodized Ti foil coated with Ir (light green).

the curve becomes hysteretic due to the increased capacitance concomitant with the increased surface area of the electrode.

Let us now focus on the influence of the iridium catalyst loading on the performance toward OER. Atomic layer deposition permits a systematic control of the catalyst loading, even at low coating thicknesses. Figure 5 demonstrates the dependence of the steady-state current density J (measured after 1 h for equilibration) on the number of ALD cycles for TiO_2 tube length of $L = 12 \mu\text{m}$ at an applied overpotential of $\eta = 0.34 \text{ V}$. Note that no compensation for the ohmic resistances of samples and electrolytes is applied (an exemplary cyclic voltammogram with and without resistance compensation is presented in Figure S2 in the Supporting Information). For a first reference point, we begin with 250 ALD cycles, which

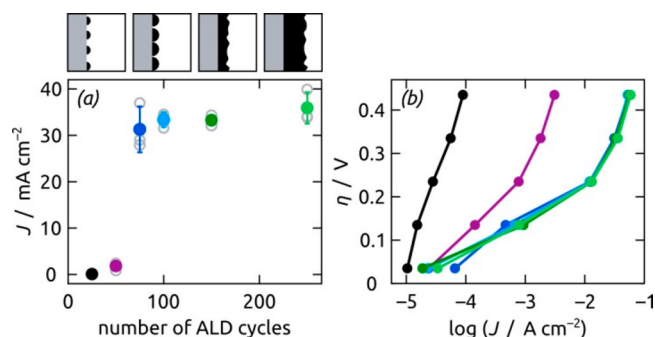


Figure 5. (a) Dependence of the current density J on the number of ALD cycles of an electrode with a TiO_2 tube length of $L \approx 12 \mu\text{m}$. J was obtained from steady-state electrolysis at $\eta = 0.34 \text{ V}$ in acidic media. Individual data points are given in gray empty circles, their averages in full disks: 25 cycles (black), 50 cycles (purple), 75 cycles (dark blue), 100 cycles (light blue), 150 cycles (dark green), and 250 cycles (light green). The panels above the graph sketch how the specific surface area of catalyst (in black) varies with the nominal coating thickness. (b) Corresponding Tafel plot comparing the performance at different overpotentials η between +0.04 and +0.44 V (values determined after 1 h equilibration time at each η).

correspond to a layer thickness of about 22 nm and are known from the literature to yield electrocatalytic activity.⁷ With the current system nanostructured Ir/ TiO_2 electrodes we obtain a current density of $J = 35.9 \pm 3.4 \text{ mA cm}^{-2}$ with the same loading (a 2-fold improvement with respect to the literature value). Similar values of J are achieved with 150, 100, and 75 cycles, which correspond to thicknesses of about 13, 9, and 6 nm, respectively. In other words, reducing the catalyst loading by a factor 3 leads to almost no loss in catalytic turnover toward OER. This behavior is logical as these relatively thick coatings are continuous. In this case, various thicknesses all present the same geometric surface area. Their ohmic resistances vary but are not relevant on the conductive TiO_2 substrate. However, the situation changes upon reducing the catalyst loadings to 50 and 25 cycles (formally 4 and 2 nm), respectively. Here, a prominent activity loss is observed, corresponding to the reduction in surface area of individual crystallites on the TiO_2 surface (see sketches above Figure 5a). The loss of film continuity for small numbers of ALD cycles has been demonstrated in similar TiO_2 tubes in the past.¹⁵ An additional effect may be due to the contribution of the (continuous) metal layer to electrical conduction along the tube length, which is lost when the layer is too thin to provide a continuous conduction path. The Tafel plot in Figure 5b reflects the same observation at lower overpotentials. The best sample exhibits a Tafel slope of approximately 90 mV per decade at $\eta < 0.2 \text{ V}$ and 200 mV per decade at $\eta > 0.2 \text{ V}$. The slopes of our nanostructured electrodes are significantly larger than other reported Ir/ IrO_2 electrodes, especially at large overpotentials,^{16–19} which is due to the prevailing transport limitation in this highly porous system. Note that at the highest current densities obtained here, the ohmic drop can be as large as 200 mV for the thinnest Ir coatings (an effect which has not been artificially compensated for in our data).

Our preparative method allows us to study the influence of the electrode's geometric surface area on the electrocatalytic water oxidation performance. Figure 6a shows the current density as a function of the nanotube length at $\eta = 0.34 \text{ V}$. The current increases upon tube elongation from 1 to 12 μm , since longer TiO_2 tubes exhibit a higher specific surface area. The

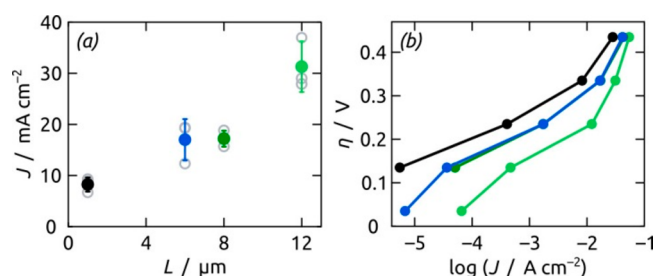


Figure 6. (a) Dependence of the current density J on the length of the TiO_2 nanotubes of an electrode coated with 75 ALD cycles of iridium. J was obtained from steady-state electrolysis at $\eta = 0.34 \text{ V}$ in acidic media. Individual data points are given in gray empty circles, their averages in full circles: $1 \mu\text{m}$ (black), $6 \mu\text{m}$ (dark blue), $8 \mu\text{m}$ (dark green), and $12 \mu\text{m}$ (light green). (b) Corresponding Tafel plot resulting from the averaged values obtained for the different tube lengths at η between $+0.04$ and $+0.44 \text{ V}$ (values determined after 1 h equilibration time at each η).

Tafel plot in Figure 6b demonstrates a qualitatively similar behavior at all overpotentials. The increase of current density with tube length is, however, largest for low overpotentials. Indeed, the higher the overpotential, the more strongly mass and charge transport limit turnover for the longest tubes.

After all electrochemical investigations, the cyclic voltammetry curves are identical to those recorded before them, hinting that the microstructure of our electrodes is maintained (Figure S3 in the Supporting Information). This assumption is further substantiated by scanning electron microscopy (Figure S4). Furthermore, the evolution of dioxygen can be demonstrated with an optical oxygen sensor during steady-state electrolysis. Degassing the electrolyte with nitrogen gas before the electrochemical performance and a sealed measurement setup prevent the system from any oxygen contamination from air. Figure S5 in the Supporting Information shows the time-dependent increase of the dissolved oxygen concentration in the electrolyte solution and the corresponding steady-state current density at $\eta = 0.34 \text{ V}$ over an electrolysis lasting 1 h. The Faradaic efficiency cannot be determined from these data, given that only a small fraction of the oxygen produced remains dissolved in the electrolyte, as the main part is released in gaseous form (as indicated by bubbles rising through the electrolyte).

The 10 mA cm^{-2} performance is often taken as a benchmark for the activity toward OER: the lower the overpotential η needed to reach this current density, the better the catalyst and the electrode. To reach 10 mA cm^{-2} , most state-of-the-art electrodes require $\eta > 0.30 \text{ V}$. With our nanostructured Ir/TiO_2 electrodes (coated with 75 ALD cycles) we are already able to achieve current densities of $J = 12.2 \text{ mA cm}^{-2}$ at $\eta = 0.24 \text{ V}$. This value also improves on the similar system based on Ir ALD on anodic alumina, previously reported,⁷ by $\eta = 0.10 \text{ V}$. Table 2 presents a comparison of the activity achieved with various electrodes based on iridium (or iridium oxide) in acidic conditions.

Another relevant performance parameter is the mass activity, for which the state of the art is 99.6 A g^{-1} at $\eta = 0.28 \text{ V}$ and 135.83 A g^{-1} at $\eta = 0.30 \text{ V}$.^{17,27} For our electrode with a tube length of $L = 12 \mu\text{m}$ coated with 75 ALD cycles of iridium, a catalyst loading of $160 \mu\text{g cm}^{-2}$ was determined via ICP-OES analysis. This loading yields an activity of 200 A g^{-1} at an overpotential of $\eta = 0.34 \text{ V}$, which renders our system competitive with the state of the art.

Table 2. Comparison of the OER Performance at the Benchmark Value of 10 mA cm^{-2} of Our Nanostructured Ir/TiO_2 Electrodes with State of the Art

electrode	overpotential at 10 mA cm^{-2} in V	ref
our Ir/TiO_2	< 0.24	this work
Ir/AAO	0.34	7
$\text{IrO}_2/\text{TiO}_2$	> 0.40	20
IrO_x film Ti cylinders	≥ 0.37	21
IrO_x/Ti	≥ 0.27	22
IrO_2 NP	0.42	23
IrO_2 nanoneedles	0.313	24
Ir nanocluster	0.37	25
Ir thin film	0.34	26

CONCLUSIONS

We have established a preparative strategy toward water oxidation electrodes with extraordinary electrocatalytic proficiency. We generate a large specific surface area via anodization of a metallic substrate. In contrast to classical carbon black substrates (or similar), the geometry of the porous substrate is highly ordered and controlled, which ensures that every noble metal particle is accessible to the electrolytic solution. The capability of systematically varying the tube geometry (based on the anodization conditions) and the noble metal coating thickness (with the number of ALD cycles performed) as two independent parameters allows us to optimize the iridium loading. Correspondingly, we reach the benchmark current density of 10 mA cm^{-2} at a very low overpotential value slightly below 0.24 V . Our porous system is limited by mass and charge transport at large overpotentials and therefore cannot sustain very large current densities. It is, however, highly proficient at low overpotentials, where moderate but practically relevant current densities can be sustained with a high level of reversibility. At 10 mA cm^{-2} , for example, our applied potential value ($E = 1.47 \text{ V}$ vs RHE) corresponds to a 16% energy loss with respect to the energy stored chemically (thermodynamic potential $E^\circ = 1.23 \text{ V}$). Thus, the energy conversion efficiency reached is almost 85%,

$$\text{eff} = \frac{\text{chemical energy stored}}{\text{electrical energy input}} = \frac{qE^\circ}{q(E^\circ + \eta)} = \frac{E^\circ}{E^\circ + \eta} = \frac{1.23 \text{ V}}{1.47 \text{ V}} = 0.84$$

EXPERIMENTAL SECTION

Materials. Chemicals were purchased from Strem, Sigma-Aldrich, and VWR and used as received. Ti foils (99.6%, 0.1 mm thick) were obtained from Advent Materials.

Preparation of TiO_2 Nanotubes. TiO_2 nanotubes were grown from Ti foils with a size of approximately 5 cm^2 . The Ti foils were cleaned in successive soap/water, isopropanol, and acetone baths under sonication for 15 min. After drying in a nitrogen flow, the Ti foils were placed in a homemade PVC beaker with a circular opening and held between an O-ring and a copper plate serving as the electrical contact. The beaker was closed with a metal housing equipped with a silver wire as the counter electrode and a mechanical stirrer. The electrochemical oxidation (anodization) was carried out in ethylene glycol containing 5% H_2O and 0.5 wt % NH_4F at $+60 \text{ V}$ for 1, 2, and 3 h. Subsequently, the Ti foils were rinsed with distilled water and dried at 45°C . The sacrificial TiO_2 layer was removed in 20% acetic acid under sonication for 5 min. Further, Ti foils were anodized in 50% glycerol, 50% H_2O , and 0.5 wt % NH_4F at $+25 \text{ V}$ for 30 min and finally rinsed with distilled water and dried at 45°C . The Ti foils were then annealed at 450°C for 4 h in air in a muffle furnace from Nabertherm. Finally, the TiO_2 tubes were coated with iridium by atomic layer deposition using a Gemstar-6 ALD reactor from

Arradiance. Ethylcyclopentadienyl-1,3-cyclohexadiene-iridium(I) ((EtCp)Ir(CHD)) and ozone were used as precursors. The deposition was carried out at 220 °C, whereas the iridium precursor was heated to 90 °C and ozone was produced from oxygen in an ozone generator model BMT803N from BMT Messtechnik.

Electrochemical Studies. For the electrochemical investigation, the samples were cut into small pieces and glued onto copper plates using double-sided copper tape. In order to define an accurate electrode surface area, a mask made of polyimide tape (Kapton) with a circular opening of $d = 2.0$ mm was used. The electrochemical studies were performed in a three-electrode setup using a Pt mesh as the counter electrode and a Ag/AgCl reference electrode with a standard redox potential of +0.20 V vs NHE. Cyclic voltammetry and steady-state electrolysis were recorded in 0.1 M H₂SO₄ using a Gamry Interface 1000 potentiostat. Cyclic voltammograms were recorded starting at the open circuit potential between 0.0 V and +1.4 V vs Ag/AgCl. For steady-state electrolyses, several applied potential values were chosen between $E = 1.10$ and 1.50 V ($\eta = 0.04$ and 0.44 V) and maintained for 1 h before the current values were determined. Direct quantification of the evolved dioxygen was performed with an oxygen sensor model Visiferm DO 160 by Hamilton.

Characterization. The geometry and morphology of the nanostructured samples were characterized by scanning electron microscopy using GeminiSEM 500 from Zeiss. The crystal structure was analyzed on Bruker D8 Advance equipped with a Cu K α source and LynxXE XE T detector. The iridium catalyst loading was determined via inductively coupled plasma optical emission spectrometry ICP-OES using Optima 8300, PerkinElmer. For the analysis four-point calibrations were performed by diluting certified standards.

■ ASSOCIATED CONTENT

Supporting Information

The Supporting Information is available free of charge on the ACS Publications website at DOI: 10.1021/acsaem.9b00402.

Figures S1–S5 of scanning electron micrographs, cyclic voltammograms, and dioxygen evolution (PDF)

■ AUTHOR INFORMATION

Corresponding Author

*E-mail: julien.bachmann@fau.de.

ORCID

Julien Bachmann: 0000-0001-6480-6212

Author Contributions

The manuscript was written through contributions of all authors. All authors have given approval to the final version of the manuscript.

Notes

The authors declare no competing financial interest.

■ ACKNOWLEDGMENTS

This research was funded by the German Federal Ministry of Education and Research (Bundesministerium für Bildung und Forschung, BMBF) via the project TubulAir (Project 03SF0436G) and by the European Research Council with an ERC Consolidator Grant (Grant 647281, “Solacylin”). We thank Dr. S. Bochmann for SEM analysis and P. Hoppe for ICP-OES analysis.

■ REFERENCES

(1) Reier, T.; Nong, H. N.; Teschner, D.; Schlögl, R.; Strasser, P. Electrocatalytic Oxygen Evolution Reaction in Acidic Environments – Reaction Mechanisms and Catalysts. *Adv. Energy Mater.* **2017**, *7*, 1601275.

(2) Anderson, D.; Leach, M. Harvesting and redistributing renewable energy: on the role of gas and electricity grids to overcome intermittency through the generation and storage of hydrogen. *Energy Policy* **2004**, *32*, 1603–1614.

(3) Pourbaix, M. J. N.; Van Muylder, J.; de Zoubov, N. Electrochemical Properties of the Platinum Metals. *Platinum Met. Rev.* **1959**, *3*, 47–53.

(4) Alia, S. M.; Rasimick, B.; Ngo, C.; Neyerlin, K. C.; Kocha, S. S.; Pylypenko, S.; Xu, H.; Pivovar, B. S. Activity and Durability of Iridium Nanoparticles in the Oxygen Evolution Reaction. *J. Electrochem. Soc.* **2016**, *163*, F3105–F3112.

(5) Carmo, M.; Fritz, D. L.; Mergel, J.; Stolten, D. A comprehensive review on PEM water electrolysis. *Int. J. Hydrogen Energy* **2013**, *38*, 4901–4934.

(6) Haschke, S.; Pankin, D.; Petrov, Y.; Bochmann, S.; Manshina, A.; Bachmann, J. Design Rules for Oxygen Evolution Catalysis at Porous Iron Oxide Electrodes: A 1000-Fold Current Density Increase. *ChemSusChem* **2017**, *10*, 3644–3651.

(7) Schlicht, S.; Haschke, S.; Mikhailovskii, V.; Manshina, A.; Bachmann, J. Highly Reversible Water Oxidation at Ordered Nanoporous Iridium Electrodes Based on an Original Atomic Layer Deposition. *ChemElectroChem* **2018**, *5*, 1259–1264.

(8) Mor, G. K.; Varghese, O. K.; Paulose, M.; Shankar, K.; Grimes, C. A. A review on highly ordered, vertically oriented TiO₂ nanotube arrays: Fabrication, material properties, and solar energy applications. *Sol. Energy Mater. Sol. Cells* **2006**, *90*, 2011–2075.

(9) Mor, G. K.; Shankar, K.; Paulose, M.; Varghese, O. K.; Grimes, C. A. Use of Highly-Ordered TiO₂ Nanotube Arrays in Dye-Sensitized Solar Cells. *Nano Lett.* **2006**, *6*, 215–218.

(10) Nakata, K.; Fujishima, A. TiO₂ photocatalysis: Design and applications. *J. Photochem. Photobiol., C* **2012**, *13*, 169–189.

(11) Park, J. H.; Kim, S.; Bard, A. J. Novel Carbon-Doped TiO₂ Nanotube Arrays with High Aspect Ratios for Efficient Solar Water Splitting. *Nano Lett.* **2006**, *6*, 24–28.

(12) Roy, P.; Berger, S.; Schmuki, P. TiO₂ Nanotubes: Synthesis and Applications. *Angew. Chem., Int. Ed.* **2011**, *50*, 2904–2939.

(13) Aaltonen, T.; Ritala, M.; Sammelselg, V.; Leskela, M. Atomic layer deposition of iridium thin films. *J. Electrochem. Soc.* **2004**, *151*, G489–G492.

(14) Haemäläinen, J.; Kemell, M.; Munnik, F.; Kreissig, U.; Ritala, M.; Leskelä, M. Atomic layer deposition of iridium oxide thin films from Ir(acac)₃ and ozone. *Chem. Mater.* **2008**, *20*, 2903–2907.

(15) Schlicht, S.; Barr, M. K. S.; Wu, M.; Hoppe, P.; Spiecker, E.; Peukert, W.; Bachmann, J. Minimization of Catalyst Loading on Regenerative Fuel Cell Positive Electrodes Based on Titanium Felts using Atomic Layer Deposition. *ChemElectroChem* **2018**, *5*, 3932–3937.

(16) Reier, T.; Oezaslan, M.; Strasser, P. Electrocatalytic Oxygen Evolution Reaction (OER) on Ru, Ir, and Pt Catalysts: A Comparative Study of Nanoparticles and Bulk Materials. *ACS Catal.* **2012**, *2*, 1765–1772.

(17) Lettenmeier, P.; Majchel, J.; Wang, L.; Saveleva, V. A.; Zafeiratos, S.; Savinova, E. R.; Gallet, J. J.; Bournel, F.; Gago, A. S.; Friedrich, K. A. Highly active nano-sized iridium catalysts: synthesis and operando spectroscopy in a proton exchange membrane electrolyzer. *Chem. Sci.* **2018**, *9*, 3570–3579.

(18) Oaktan, E.; Lebedev, D.; Povia, M.; Abbott, D. F.; Fabbri, E.; Fedorov, A.; Nachttegaal, M.; Coperet, C.; Schmidt, T. J. IrO₂-TiO₂: A High-Surface-Area, Active, and Stable Electrocatalyst for the Oxygen Evolution Reaction. *ACS Catal.* **2017**, *7*, 2346–2352.

(19) Cherevko, S.; Geiger, S.; Kasian, O.; Mingers, A.; Mayrhofer, K. J. J. Oxygen evolution activity and stability of iridium in acidic media. Part 1. – Metallic iridium. *J. Electroanal. Chem.* **2016**, *773*, 69–78.

(20) Shi, Y.; Lu, Z.; Wang, Z.; Guo, C.; Tan, H.; Yan, C. Fabrication of IrO₂ decorated vertical aligned self-doped TiO₂ nanotube arrays for oxygen evolution in water electrolysis. *Int. J. Hydrogen Energy* **2018**, *43*, 9133–9143.

(21) Reier, T.; Teschner, D.; Lunkenbein, T.; Bergmann, A.; Selve, S.; Kraehnert, R.; Schlögl, R.; Strasser, P. Electrocatalytic Oxygen

Evolution on Iridium Oxide: Uncovering Catalyst-Substrate Interactions and Active Iridium Oxide Species. *J. Electrochem. Soc.* **2014**, *161*, F876–F882.

(22) Cherevko, S.; Reier, T.; Zeradjanin, A. R.; Pawolek, Z.; Strasser, P.; Mayrhofer, K. J. J. Stability of nanostructured iridium oxide electrocatalysts during oxygen evolution reaction in acidic environment. *Electrochem. Commun.* **2014**, *48*, 81–85.

(23) Lee, Y.; Suntivich, J.; May, K. J.; Perry, E. E.; Shao-Horn, Y. Synthesis and Activities of Rutile IrO₂ and RuO₂ Nanoparticles for Oxygen Evolution in Acid and Alkaline Solutions. *J. Phys. Chem. Lett.* **2012**, *3*, 399–404.

(24) Lim, J.; Park, D.; Jeon, S. S.; Roh, C.-W.; Choi, J.; Yoon, D.; Park, M.; Jung, H.; Lee, H. Ultrathin IrO₂ Nanoneedles for Electrochemical Water Oxidation. *Adv. Funct. Mater.* **2018**, *28*, 1704796.

(25) Pi, Y.; Shao, Q.; Wang, P.; Guo, J.; Huang, X. General Formation of Monodisperse IrM (M = Ni, Co, Fe) Bimetallic Nanoclusters as Bifunctional Electrocatalysts for Acidic Overall Water Splitting. *Adv. Funct. Mater.* **2017**, *27*, 1700886.

(26) McCrory, C. C. L.; Jung, S.; Ferrer, I. M.; Chatman, S. M.; Peters, J. C.; Jaramillo, T. F. Benchmarking Hydrogen Evolving Reaction and Oxygen Evolving Reaction Electrocatalysts for Solar Water Splitting Devices. *J. Am. Chem. Soc.* **2015**, *137*, 4347–4357.

(27) Oh, H.-S.; Nong, H. N.; Reier, T.; Gliech, M.; Strasser, P. Oxide-supported Ir nanodendrites with high activity and durability for the oxygen evolution reaction in acid PEM water electrolyzers. *Chem. Sci.* **2015**, *6*, 3321–3328.